CHAPTER 1

Motivation and Background

1.1 Nanotechnology and Nanostructures

Nanotechnology has been considered as an innovation technology that is anticipated to have a great impact on the scientific community, medicine and industrial revolution [1, 2]. Nanotechnology [1-4] is using devices or engineered materials with the functional organization to be technologies on the nanometre scale of volume, that the one billionth of a metre, that is typically ranging from the scale of range about 1 nanometres to 100 nanometres of a metre in at least one dimension. This implies that some characteristic of the material or device is able to be worked by chemical and/or physical at nanometre resolutions. The functional of nanomaterial properties effect are unique to the new technology which it cannot find in constituent elements [1-4]. For example, nanowires that were electrically conducting have potential for apply in the nanoelectronic devices [5, 6]. There are from a synthesis of nanotechnologies two classifier as variations of bottom-up technologies and top-down technologies in **Fig.1.1**, such as self-assembly and lithographic methods, respectively. The Bottom-up methods [7-9] begin with the point of one or extra defined the molecular class, which refer to the certain procedures that the end of the result in a higher-ordered and the organized structure. The Top-down [7-9] begins the material originate with a bulk material that all was integrated nanoscale details.

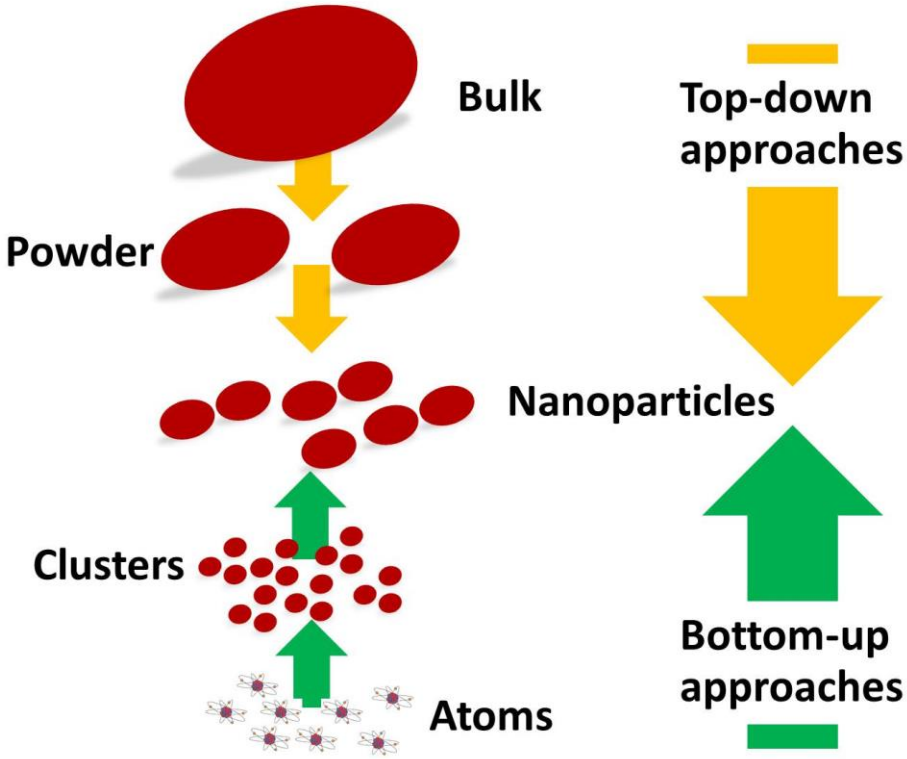

Figure 1.1 The sematic diagram of a synthesis of nanotechnologies two classifier as variations of bottom-up technologies and top-down technologies.

Nanostructures [10-12] are materials that synthesized to be some structures on the nanometre scale by a synthesis of nanotechnologies, such as nanowires, nanoparticles, nano-rods and nanotubes. They are included nanomaterials (the materials which have a single unit sized between 1-1000 nanometres in at least one dimension) to be form structure such as molecular, they have intermediate size between molecular and microscopic (micrometer-sized) structures in **Fig 1.2**.

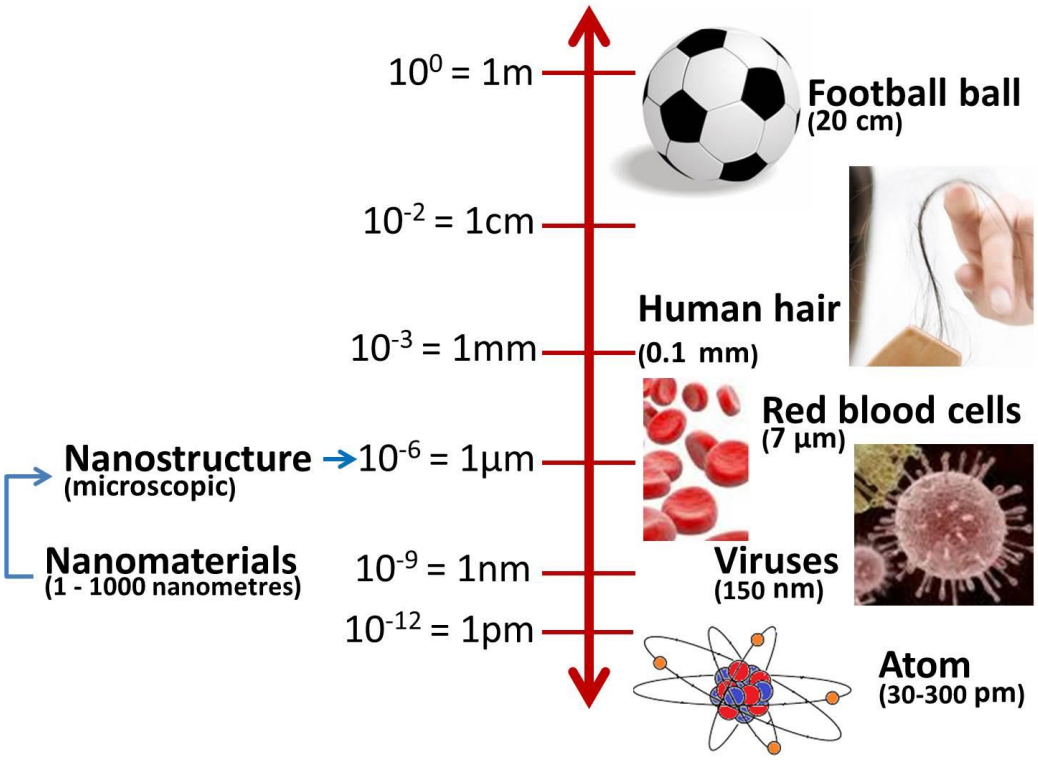

Figure 1.2 Examples of nanostructures and nanomaterials with their typical ranges of dimension [7-9].

This is mainly due to the novel properties of nanomaterials resulting from reduction in size that could open for new generations of nanodevices a wide range of applications [13-15]. In addition, nanostructures or shapes of nanomaterials also play an important role for this emerging development.

1.2 Zinc oxide polymorphs

ZnO is one of the II−VI semiconductors group [4] that is metal oxide a wide band gap semiconductor and generally crystallizes in formation either the hexagonal that wurtzite structure or cubic Zn blende. The ZnO hexagonal that wurtzite structure was the most stable at ZnO ambient conditions with crystals composed Zn^{2+} and O^{2-} ions plans stacked alternately in accordance with the *c*-axis in the **Fig. 1.3(a)**. The hexagonal structured ZnO has property that include the space group P63mc, a point of group 6mm (Hermann-Mauguin notation), and the lattice constants of ZnO are *a* as *b* as 3.25 Å and

c as 5.2 Å; their ratio of *c*/*a* about as 1.60 is close to the ideal of value for hexagonal structure cell of *c*/*a* as 1.633.

An ideal in the ZnO Bulk, nanostructures and the thin films about wurtzite crystal structure ZnO was reported by Jagadish et al. [16]. The axial ratio of *c*/a and the *U* parameter which was a admeasure of the number by which each the atom was displaced with discuss to the next in accordance with direction of the *c*-axis, were interrelated which the relationship of the equation, $Uc/a = (3/8)^{1/2}$, with ratio of $c/a = (8/3)^{1/2}$ and the *U* as 3/8 for an ideal crystal in **Fig. 1.3(b).** This ideal arrangement of ZnO crystals deviate by changing the both of these values of crystals. This deviation happen such which the tetrahedral of distances were reserved roughly constant in the lattice. For the ZnO wurtzite structure, the experimentally of the real values of *U* and the ratio of *c*/*a* were determined in the range of *U* as 0.3817–0.3856 and the ratio of *c*/*a* as 1.593–1.6035". The basic physical ZnO properties were shown in **Table 1.1.**

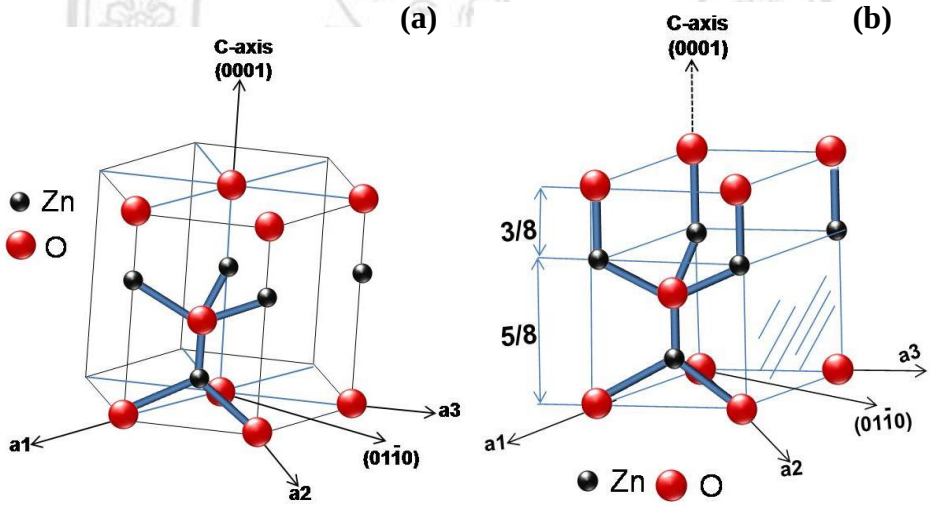

Figure 1.3 (a) The hexagonal ZnO wurtzite structure (b), dimension and direction of the ZnO unit cell structure.

Table 1.1 the elementary physical properties of ZnO.[17-19]

Properties	Volume
Average atomic number	19
Average atomic weight	40.69
Coefficient of linear thermal expansion:	
along the direction of *c*-axis (1/K)	2.9×10^{-6}
across the direction of *c* axis (1/K)	4.8×10^{-6}
Debye temperature (K)	416
Density ($g\cdot cm^{-3}$)	5.6803
Enthalpy of formation (298K) ($kJ\cdot mol^{-1}$)	-350.5
Enthalpy of fusion ($kJ\cdot mol^{-1}$)	52.30
Electron mobility ($cm^2\cdot V^{-1}\cdot s^{-1}$)	1000
Index of refraction (632.8 nm)	2.0041
Melting point (K)	2,248
Specific heat at room temperature, constant pressure ($J\cdot g^{-1}K^{-1}$)	0.494
Static dielectric constant:	
along the *c*-axis	8.75
across the *c*-axis	7.8

1.2.1 Growth kinetics of ZnO nanostructures

The ZnO polymorphs was reported by Zhong Lin Wang[20] an ideal classical ZnO growth structures. It has triple formation of rapid growth of directions: $<0\bar{1}\,\bar{1}0>(\pm[01\bar{1}0], \pm[10\bar{1}0], \pm[1\bar{1}00])$; $<2\bar{1}\,\bar{1}0>$ $(\pm[2\bar{1}\,\bar{1}0], \pm[\bar{1}2\bar{1}0], \pm[\bar{1}\,\bar{1}20])$; and $\pm[0001]$. Jointly with the polar of surfaces because of the atomic closes, ZnO displays an extensive range of unique structures that able to be grown by tuning the growth rates lengthwise these directions. The one of the most reflective the factors defining the morphology comprises with the relative of the surface happenings of numerous growth of the facets under specified conditions. Macroscopically, the ZnO crystal structure has diverse kinetic of the parameters for diverse crystal structure planes in **Fig 1.4**, which were emphasized under controlled growth conditions.

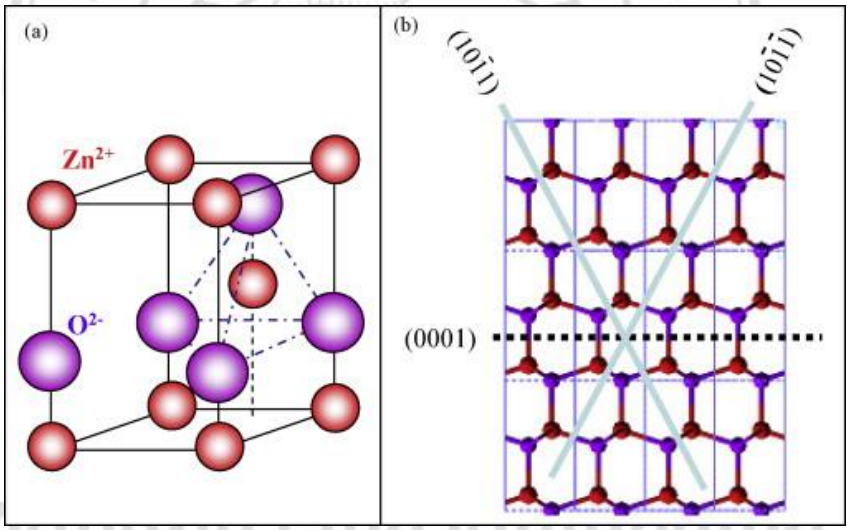

Figure 1.4 ZnO Wurtzite structure model was presented in (a), and (b) The ZnO nanostructures have three types of facets. Reprinted with permission from ref[20]. Copyright (2009) Elsevier.

Thus, once the first period of the nucleation and the incubation, the crystallite shall normally improve into a triple -dimensional objective with well-defined, low index of the crystallographic surfaces. A small typical growth of morphologies was shown in **Fig. 1.4(a)–(c)** of 1D ZnO nanostructures. These ZnO structures tend to capitalize on the areas of the plan of $\{01\bar{1}0\}$ and $\{2\bar{1}\,\bar{1}0\}$ sides due to has the lower of the energy. The Polar-nanobelt morphology exposed in **Fig. 1.4(b)** was controlled typical growth by

the polar of surfaces. It able to be grows by presenting of the planar defects that parallel to the polar of the surfaces. The planar defects and doubles were detected infrequently parallel to the (0001) direction of lane, but locomotion was barely seen."

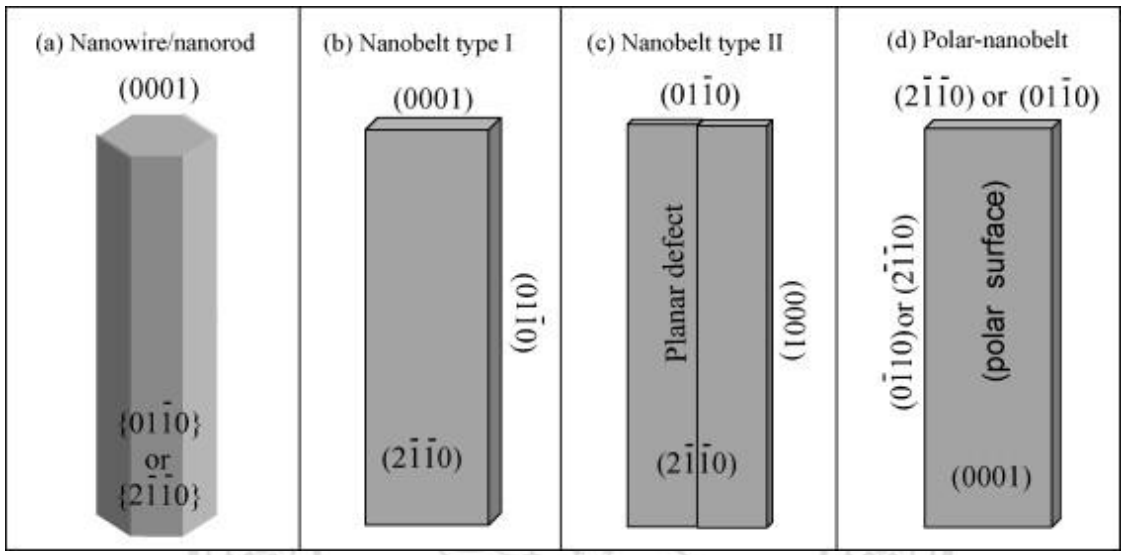

Figure 1.5 One-dimensional ZnO nanosturctures have typical growth morphologies and the corresponding facets. Reprinted with permission from ref[20]. Copyright (2009) Elsevier.

ZnO nanosturctures has caught attention due to their wide variety of structures or morphologies such as nanobelts[21], nanoparticles [22], nanowires[23, 24], nanorings [20, 25], and tetrapods[26, 27], which perhaps the amusing the family between all materials in both properties and the structures. For over the past decade, the ZnO nano-engineering[28] by controlling its size and morphology using various synthetic techniques has been executed and a great variety of morphologies of ZnO nanostructured [10, 20, 29] has been accomplished. The morphological variety of ZnO nanostructured leads to some interesting properties including opto-electrical properties[30-32] and surface-related [33]. Thus, the growth kinetics of synthetic process need to control by nano-engineering was an important issue for utilizing ZnO nanostructures [10, 34, 35].

1.2.2 ZnO tetrapod-like features

Basic Properties of ZnO tetrapods **(Fig.1.6)** was reported by N. Hongsith et al.[36] an ideal growth kinetics and model of ZnO tetrapods that "generally, the growth mechanism of ZnO nanostructures such as, the belt-like, and wire-like can be explained by a vapor-solid mechanism for the kinetics of anisotropic growth mechanism at equation (1) [36].

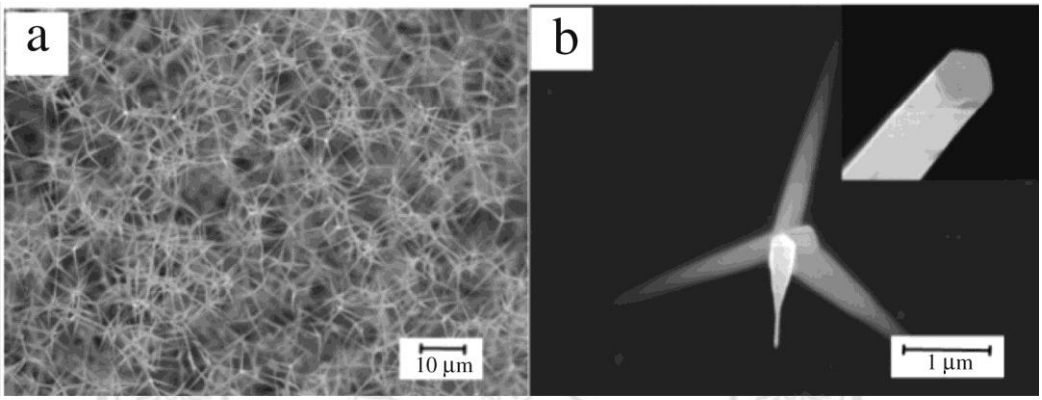

Figure 1.6 FE-SEM images of T-ZnO were synthesized by the thermal oxidation with (a) the all of them of magnification of ×1000 and (b) one of them of ×20,000. The inset in (b) image shows the tip of a tetrapod. Reprinted with permission from ref[36]. Copyright (2009) Elsevier.

P is the nucleation probability on the surface of a ZnO nanostructure was given by

$$P = B\exp\left(\frac{-\pi\sigma^2}{k_b^2 T^2 in(\alpha)}\right) \quad \text{.....(1.1)}$$

where B is a parameter constant.

σ is the surface energy of the solid ZnO tetrapod.

k_B is the Boltzmann's constant.

T is the absolute temperature.

α is the supersaturation ratio between the actual vapor pressure and the equilibrium vapor pressure corresponding to temperature (usually, $\alpha > 1$) [36].

In the supersaturation ratio, the growth direction of a one-dimensional nanostructure of ZnO was normally along a low crystal index such as, $\{11\bar{2}0\}, \{01\bar{1}0\}$, $\{0001\}$ etc. because of their surface energy which was related to the crystal plane index in crystal structure of ZnO. The ZnO has the lowest surface energy at $\{0001\}$ c-axis direction when σ_{min}, proposing the highest nucleation probability P. Then, the c-axis direction of the ZnO structure exhibits the highest possibility for the growth and the fastest growth rate direction.

The growth kinetics of ZnO wire-like and belt-like nanostructures was explain based on the equation of nucleation probability in the event of different supersaturation ratio. The growth of ZnO nanostructures reported before was on the substrates suggesting that the two dimensional growth kinetics. Though, the ZnO tetrapod was not grown on the substrate suggesting different growth kinetics. T-ZnO growth kinetics was three dimensional growth kinetics through growth direction still desired along the c-axis was proposed.

The ZnO tetrapods comprise with four grains having a hexagonal structure. These four grains should be resulting from the basic ZnO hexagonal structure. In **Fig. 1.7(a),** ZnO hexagonal structure a unit cell has the zinc ion that was surrounded by tetrahedra of oxygen ions and vice-versa, with a coordination number of 4:4. By since an oxygen atom as a core, in **Fig. 1.7 (b),** the tetrahedral structure could be drawn having an angle between each axis of 109.5. This tetrahedral structure was considered to be a beginning seed to form a ZnO tetrapod structure in **Fig. 1.7 (b)**. The vertexes of the tetrahedral structure were preferred nucleation places to form 3D structure because of the low surface energy in $\{0001\}$ c-axis directions. The 3D structure could form by growth and then condensation of ZnO vapor caused by supersaturation conditions, growing as ZnO tetrapod 4 legs along their $\{0001\}$c-axes, I, II, III, and IV of legs as model shown in **Fig. 1.7 (c).** These 4 legs had impinge forming 6 grain boundaries, A, B, C, D, E, F, and grain edges as shown in **Fig. 1.7 (c) and (d).”**

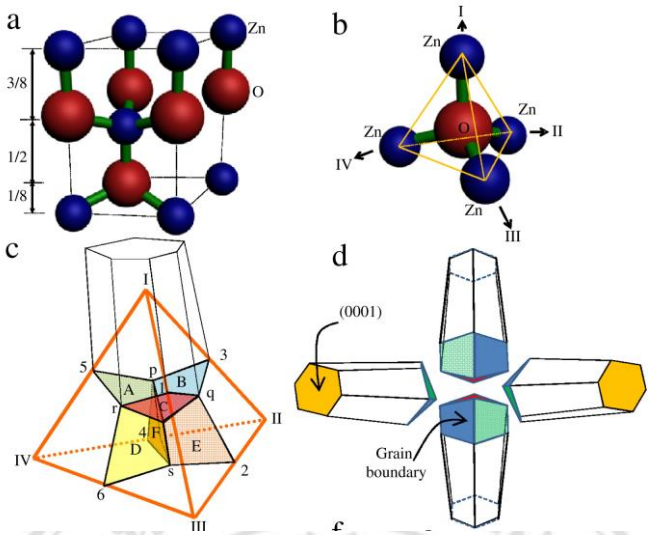

Figure 1.7 (a) Model of ZnO structure unit cell; (b) Model of Zn atom tetrahedral construction related with ZnO unit cell; (c) the grain edges and grain boundaries ZnO tetrapod nucleation image (d)T-ZnO four leg with a wedge-like shape join together and form four grain boundaries. Reprinted with permission from ref[36]. Copyright (2009) Elsevier.

1.2.3 ZnO nanostructures network

ZnO nanostructures networks have vary morphology and characteristic due to them were growth by different technique method. For example, ZnO network thin film was prepared by sputtering technique, ZnO network was prepared by vapor phase transport oxidation, ZnO nanowires and nanorod network was prepared by solid-vapor deposition and ZnO nanowall network, and tetapods network was prepared by thermal oxidation [38-40] in **Fig. 1.8**.

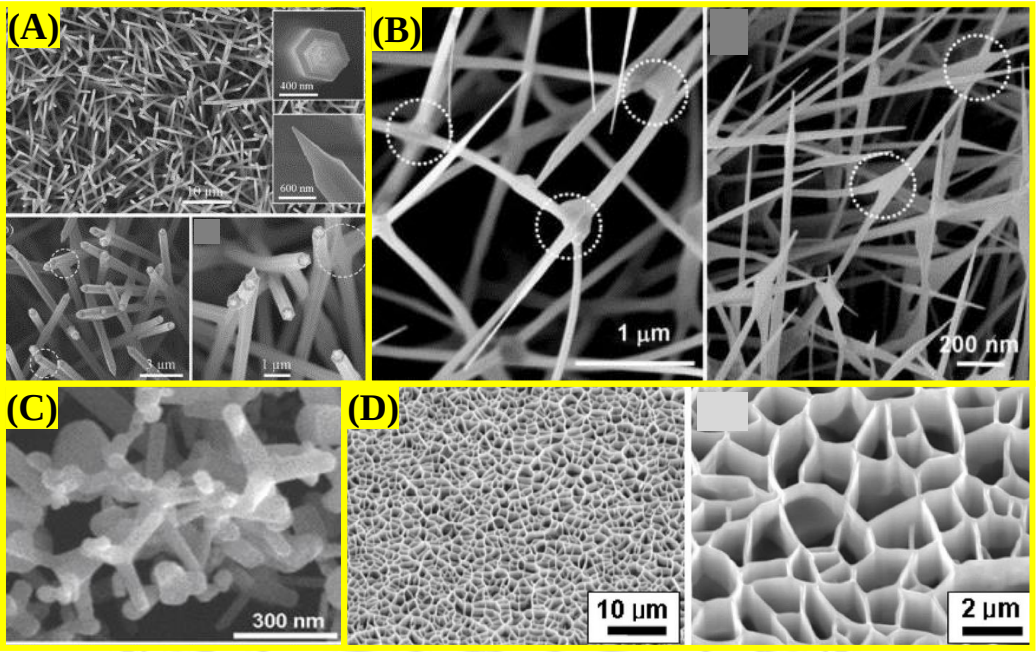

Figure 1.8 SEM image of ZnO nanostructures networks vary morphology and characteristic due to them were growth by different technique method. (A) ZnO nanorods were synthesized through a thermal evaporation process. Reprinted with permission from ref [37]. Copyright (2005) Elsevier. (B) The ZnO nanowires in the nano-network structures were synthesized by the high temperature of solid–vapor deposition technique. Reprinted with permission from ref [38]. Copyright (2005) Elsevier. (C) ZnO nano-microstructures networks were grown on the patterned chip by via B-FTS technique. Reprinted with permission from ref [39]. Copyright (2013) John Wiley and Sons. (D) ZnO nanowall networks were synthesized by subsequent growth technique. Reprinted with permission from ref [40]. Copyright (2007) AIP Publishing LLC.

The interconnecting structure characteristics of the quasi-aligned sharp of nanowire tips had high a number of connection of networking form and high of the surface area of these the unique nano-networks structure. They can applied the potential of candidate for the field emission, catalysts, filtering, and ultra-sensitive of the gas sensing[38] that above all as a chemical of sensor for sensing noxious of gases besides explosive the hydrogen gas [40].

The UV sensor example of ZnO tetrapods nanowires structures or nanoarms forming network structures and how to ZnO nanostructures networks working different

form other structures was shown by schematic diagram in **Fig.1.9**[39]. Indicating on the possible possession of more than a few types of nano-junctions amid interconnecting with interpenetrating neighbor ZnO tetrapods nanowires structures or nano-arms forming to be network bridge in the gap was explained by schematic diagram of UV sensor of ZnO nanostructures networks A just touching of the nano-arms (**Fig.1.9 a**) or partially interpenetrated of the nano-arms (**Fig.1.9c**).

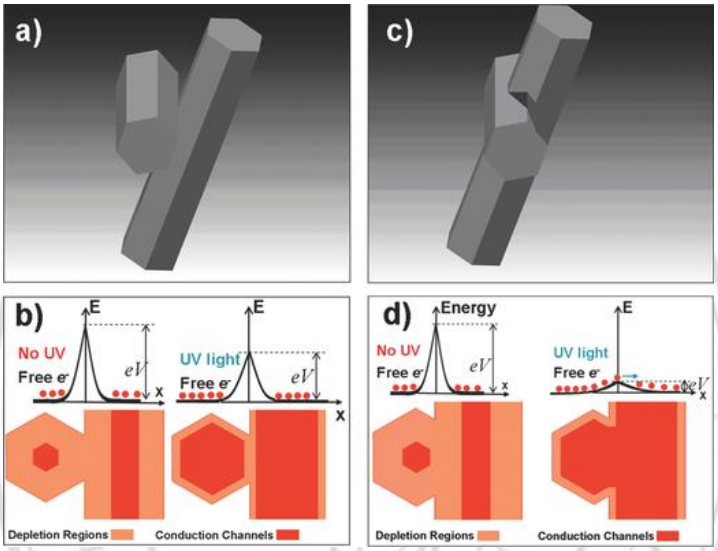

Figure 1.9 Schematic diagrams of networked ZnO nanowires; a) touching ZnO tetrapod arms, and b) it had the energy band diagram (top) and the models of cross-section connection structural the conduction mechanism of ZnO nanowires (bottom) the potentials barriers at the crystal boundary. The depletion of the electrons by desorbed the oxygen molecules on the material surface of touching ZnO nanowires effect to high the potential barrier to the material surface states. The highness of the potential barrier drops however still significantly large (top) when it was under UV illumination. c) The event of ZnO nanowires network that be the bridge in which ZnO tetrapod arms were interpenetrating of each other and d) its energy band diagram (top) and cross-section structural models of nanowires (bottom) show drops of the potential barrier at the crystal boundary. It was illuminated with the UV light (top) significantly accrete of the

channel and as a result connected of the channel (bottom). Reprinted with permission from ref[39]. Copyright (2013) John Wiley and Sons.

Electrical properties of such the nanojunctions boundary in ZnO semiconductor abled to be response for improving the electrical property activity of the interfaces among ZnO nanowire in a joining network. First, the nano-junction boundary converts an electrically active by electron trapping an extra charge of popular the carriers (e^-) at the point interface. Overall an electrons charging neutrality were designed by an electrostatic of potential barrier amid neighboring depletion layers together to the nanojunction (**Fig. 1.9 b,d**).

The **Fig. 1.9** as the bottom schematics shows the models of ZnO structural that was the conduction channel of the nano-junctions amid nanowires in the air. Interpenetrating ZnO nanowires network formations was also shown by the bottom schematics diagrams in **Fig. 1.9d**. The energy band of diagram (top) of the radiating direction of a single nanowire, indicative of the depletion area at the surface of sample, the band of surface indirect and the central section of radius in the central part of the ZnO nanostructure was also presented in **Fig. 1.9b**. As abled to be seen that the channel of conduction were still not connected, even though the dimensions channel of conduction of ZnO nanowires accrete under the UV light due to discharge of the free electrons from an oxygen ions on the zinc oxide surface (in **Fig. 1.9 b**). A high potential barrier to the zinc oxide surface conditions be existent due to the reducing electrons by an oxygen on the ZnO surface of interpenetrating ZnO nanowires. Though, the interpenetrating of ZnO nanowires forming nano-junctions via the UV irradiance had the potentials barriers that was significantly decrease and the channel distance across come to be interconnected as presents in **Fig. 1.9 d**. Different the event of other, it abled to be summarized that the UV radioactivity did not affect significantly the energy barrier among the touching zinc oxide nanowires and an electrons did not have a free conduction path. By difference, the contact that was as well intimate with a complete interpenetration would as well not great change in the conductivity under UV light as no the barrier had to be overcome. So the sensitive contact of model would be something in among a little touching and a perfect interpenetration network. As a result,

nanojunctions types formed between nanostructures in the interpenetration bridge of network had significant part in detection mechanism of such UV sensor or gas sensor.

1.3 Thermal oxidation

Thermal oxidation is the synthesis method that use oxygen reactivity with metal at high temperature to be metal oxide structures, such as ZnO nanostructure synthesis with the thermal oxidation method has been previously reported [41-44]. There are primary parameters for the thermal oxidation method, such as oxidation temperature, which are shown as follows.

ZnO nanostructures were synthesized by thermal oxidation method from zinc foils at 200−1000°C temperature range [44]. ZnO nanostructures from thermal oxidation method were shown in **Fig 1.10.** The oxidation temperature range that result of the different formation processes of ZnO nanostructures are shown in **Fig. 1.10** used to synthesis the bi-crystalline nanowire at below the melting point of Zn, nanowire the melting and boiling points of Zn, and tetrapod above the boiling point of Zn.

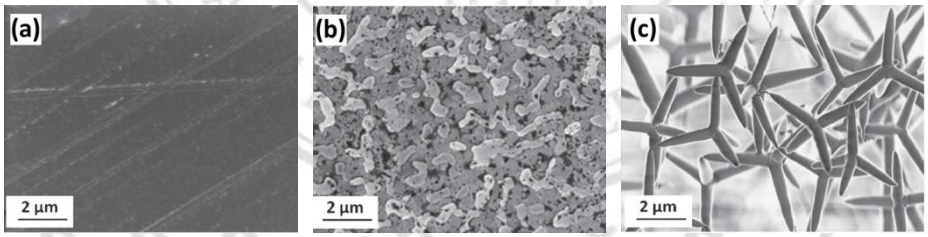

Figure 1.10 SEM images of ZnO nanostructures synthesized by oxidation temperature method at (a) 300, (b) 500, and (c) 1000oC.Reprinted with permission from ref [44]. Copyright (2014) Elsevier.

The solid−solid mechanism can be explained to conceive the formation of the bi-crystalline nanowires when oxidation temperatures relatively below the melting point of Zn (T < 400°C) that shown in the **Fig. 1.11a**. A solid ZnO coating was oxidized from solid Zn on the Zn substrate.

The liquid−solid mechanism can be explained to understand the formation of ZnO nanowires when oxidation temperature between the melting and boiling points of

Zn (420°C < T < 907°C) that shown in the **Fig. 1.11b**. First, the thin liquid Zn layer forms on the Zn substrate surface. Then, solid ZnO nucleuses were formed by reaction between the liquid layers with incoming oxygen and provide seeds for ZnO nanowire formation. After that, the ZnO nanowire grows through surface due to diffusion of Zn ions along the sidewall of the nanowire which reacting with impinging oxygen. The ZnO nanowire which the surface diffusion of Zn is driven by the concentration gradients of Zn ions along was wall from the root region to the tip. Then, most nanowires have become thinner and a coarse root at the tip since a significant amount of Zn ions was integrated into the nanowire at the root region.

The vapor–solid mechanism can be explained to understand the formation of the tetrapod when oxidation temperatures above the boiling point of Zn (T > 907°C) that shown in the **Fig. 1.11c**. First, Zn vapor was rapidly evaporated from the Zn substrate. Then, the oxidation of Zn vapor reacts with oxygen gas to be ZnO nuclei formation. Finally, an octahedral-twinned shape with exposed (0001) base planes from to be ZnO tetrapods due to the minimum of their surface energy.

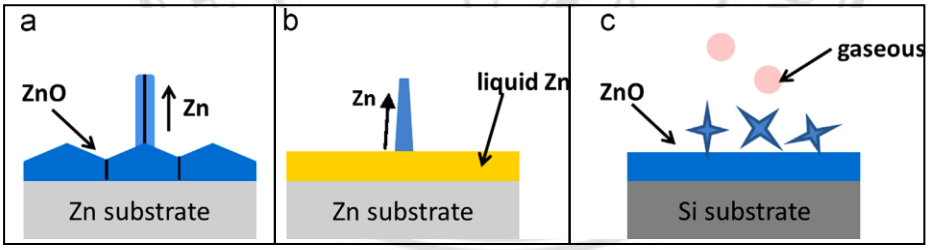

Figure 1.11 Different oxidation temperatures affect different formation processes of ZnO nanostructures: (a) Solid–solid transformation mechanism for below the melting point of Zn (b) Liquid–solid mechanism for between the melting and boiling points (c) Vapor–solid mechanism for above the boiling point of Zn. Reprinted with permission from ref [44]. Copyright (2014) Elsevier.

1.4 Microwave

The microwave is one of the electromagnetic waves. It has frequencies (f) ranging from 300 MHz to 300 GHz and wavelengths (λ) of about 1 m to 1 mm.. Following the worldwide conventions, household microwave ovens operate at frequency of about 2.45 GHz, and wavelengths (λ) of about 12.23 cm [45, 46].

1.4.1 Microwave interactions with materials

Electric field, a part of the electromagnetic wave, may be transmitted, reflected, and absorbed by materials as presented in **Fig 1.12**. Moreover, assured materials, for example the magnetic materials interact with the magnetic field element of electromagnetic waves. There are 4 typical interaction of microwave with materials that are able to be classified into the resulting interactive with microwave of categories [45, 47].

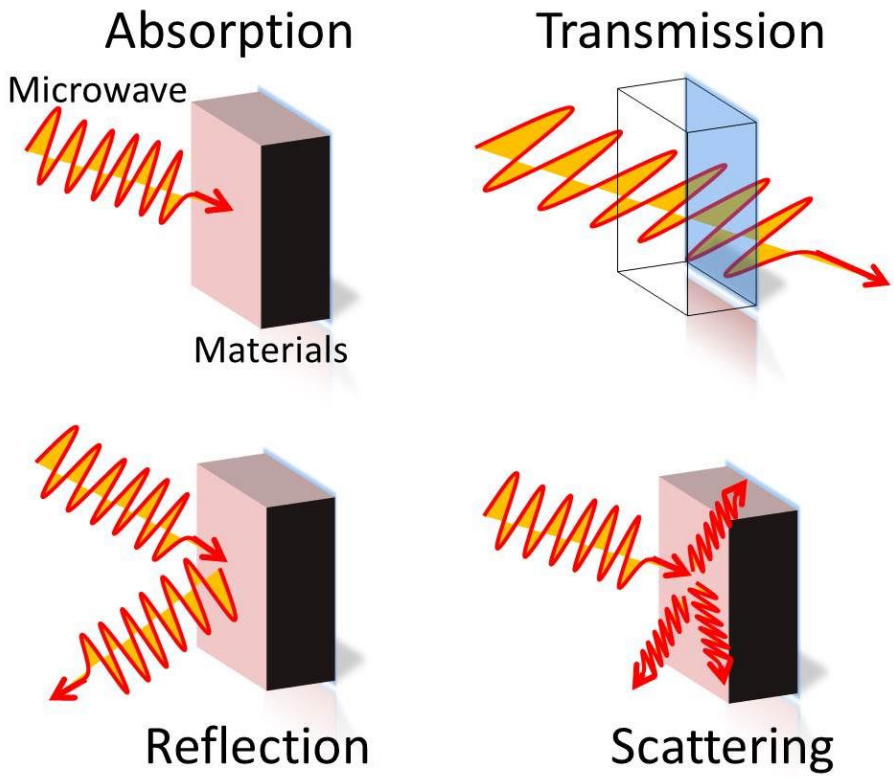

Figure 1.12 Interaction of the microwave with materials [47].

A. Opaque materials; for example metals, reproduce and do not allow electromagnetic waves to permit everywhere and typically conducting materials with free electrons.

B. Transparent materials; for example glass, ceramic ware and the air, reflect and absorb electromagnetic waves to a minor extent, permit microwave to pass through simply with tiny attenuation and low dielectric loss or insulating

C. Absorbing materials; materials which properties ranging from conductors and insulators. They absorb electromagnetic energy and change it to heat energy with great dielectric loss.

D. Magnetic materials; for example ferrites, interact with the magnetic element of electromagnetic wave and change to heat.

The microwave heating in materials can result in dielectric polarization loss as shown in **Eq. 1.4** and magnetic losses. The magnetic field effects the interaction with the electric field that both were component of the microwaves. Dielectric losses of materials are a reason of the charges redistribution and polarized under the influence of an alternating outside the electric field. The dielectric polarization losses is shown in **Eq. 1.4**[48], which includes electronic polarization, dipolar polarization, interfacial polarization and an atomic (ionic) polarization. The **Fig. 1.13** shows the different polarization of mechanisms in electric field.

In high conductive materials, for example metals, heating mechanisms depend on the conduction losses. However, in magnetic materials, heating dependson the magnetic losses, for example eddy currents, hysteresis and area wall as well as electron spin resonance. Researchers attempted to understand of microwave interaction with materials using the Maxwell equations. Moreover, they tried to analyze the electromagnetic field that was written in the equation in terms of electromagnetic potentials, as an alternative of the traditional approach in magnetic and electric the field strengths (*B* and *E*, respectively) to refer to the electromagnetic field in the microwave [47].

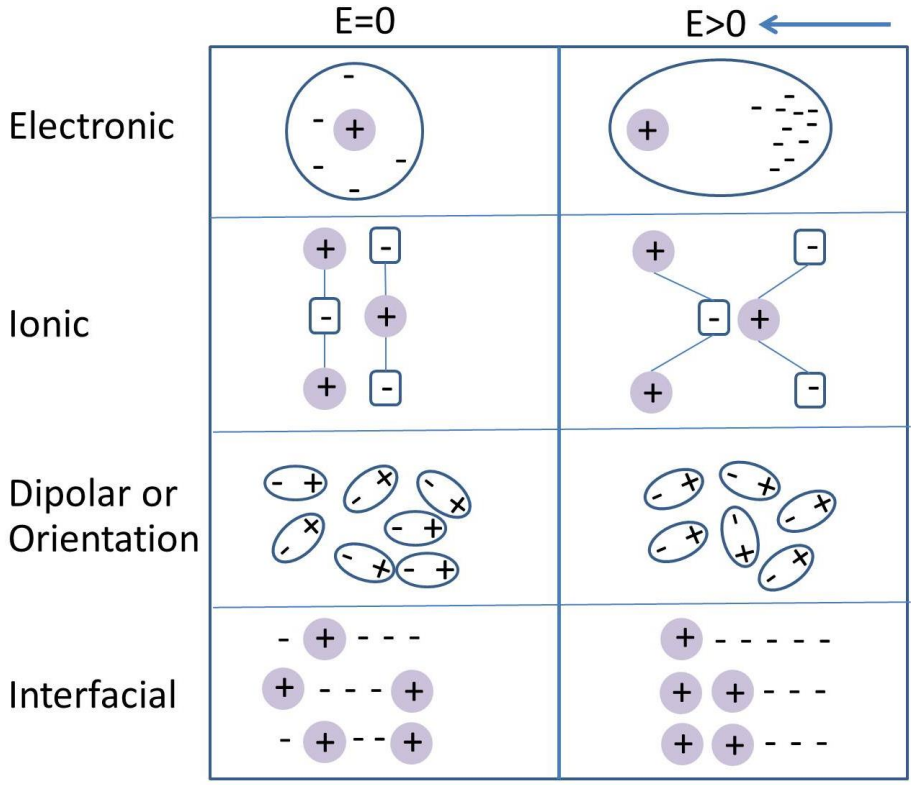

Figure 1.13 Mechanisms of charges or polarization [47].

1.4.2 Power of electromagnetic energy of the material

The phenomenon of microwave heating consists of the change of the electromagnetic energy to heat by the material. **Eq. (1.2-1.4)** expressed the power that dissipated into and/or absorbed by the material using the transformation of the electromagnetic energy into heat. The Maxwell's equations can explain phenomenon of the transformation of the electromagnetic energy addicted to heat that can be found in the some book about the microwave heating [47-51].

The equations owing to the electric losses only,

$$P_{Average\_Power} = \sigma E_{rms}^2 = \omega \varepsilon_0 \varepsilon_{eff}^{''} E_{rms}^2 = 2\pi f \varepsilon_0 \varepsilon_{eff}^{''} E_{rms}^2 = 2\pi f \varepsilon' \tan\delta E_{rms}^2 \quad \ldots.(1.2)$$

The equations owing to the magnetic losses only,

$$P_{Average\_Power} = \sigma B_{rms}^2 = \omega \mu_0 \mu_{eff}^{"} B_{rms}^2 = 2\pi f \mu_0 \mu_{eff}^{"} E_{rms}^2 \ldots\ldots\ldots\ldots\ldots\ldots (1.3)$$

The combined power equations of the material fromelectric losses and magnetic losses.

$$P_{Average\_Power} = Electric\_losses + Magnetic\_losses$$

$$P_{Average\_Power} = \omega \varepsilon_0 \varepsilon_{eff}^{"} E_{rms}^2 + \omega \mu_0 \mu_{eff}^{"} B_{rms}^2 \ldots\ldots\ldots\ldots\ldots..(1.4)$$

by

$$\tan\delta = \frac{\varepsilon^{"}}{\varepsilon^{'}}, \ldots\ldots\ldots\ldots\ldots\ldots\ldots\ldots (1.5)$$

where $\tan\delta$ refers to the loss tangent, that the efficiency of the material to convert absorbed energy into heat and describe the dielectric response.

$\varepsilon^{"}$ is the factor of dielectric loss.

$\varepsilon^{"}$ is the complicated permittivity that is a admeasure of the ability of the dielectric to absorb and supply an electrical potential energy $\tan\delta$

ω is angular frequency that formula of $\omega = 2\pi f$.

$E_{eff}^{"}$ is the root mean square of the electric field.

$\varepsilon_{eff}^{"}$ is the effective relative dielectric loss factor.

$\mu_{eff}^{"}$ is the effective relative magnetic loss factor.

The effective interrelated the dielectric loss factor is the summary of losses from the conduction and the polarization.

$$\varepsilon_{eff}^{"} = \varepsilon_{Polarization}^{"} + \varepsilon_{Conduction}^{"}$$

$$\varepsilon_{eff}^{"} = (\varepsilon_{Electronic}^{"} + \varepsilon_{Ionic}^{"} + \varepsilon_{Interfacial}^{"} + \varepsilon_{Dipolar}^{"}) + \varepsilon_{Conduction}^{"}$$

$$\varepsilon_{eff}^{"} = (\varepsilon_{Electronic}^{"} + \varepsilon_{Ionic}^{"} + \varepsilon_{Interfacial}^{"} + \varepsilon_{Dipolar}^{"}) + \varepsilon_{Conduction}^{"} \ldots\ldots\ldots\ldots (1.6)$$

1.4.3 Skin depth of materials

Skin depth or penetration depth [47-51] (d) is a dimensions of the depth of microwave penetration in a material surface. The skin depth is defined as the distance

that is measured from the material surface to a position which the incident power decays to 1/e (about 0.37) of its initial. The penetration depth is well approximated as;

$$d = \frac{1}{\alpha} = \sqrt{\frac{2}{\omega^2 \mu_0 \mu' \varepsilon_0 \varepsilon''_{eff}}} = \sqrt{\frac{2}{\omega \mu \sigma}} \quad \text{.....(1.7)}$$

where α is the attenuation factor, represented as

$$\alpha = \omega\left(\frac{\mu_0 \mu' \varepsilon_0 \varepsilon'}{2}\right)^{1/2}\left[\left(1+\left(\varepsilon''_{eff}/\varepsilon'\right)^2\right)^{1/2}-1\right]^{1/2} \text{.....(1.8)}$$

For the conductors materials, $\varepsilon''_{Polarization} = 0$, as a result **Eq. (1.6)** is reduced to

$$\sigma = \omega \varepsilon_0 \varepsilon''_{eff} = \frac{1}{\rho} \text{.....(1.9)}$$

Where σ is the conductivity of the material and ρ is the resistivity of the material. For a good conductor, resistivity = 0 and therefore the skin depth = 0. For example of the penetration depth and electrical conductivity of selected materials was shown in **Fig. 1.14**.

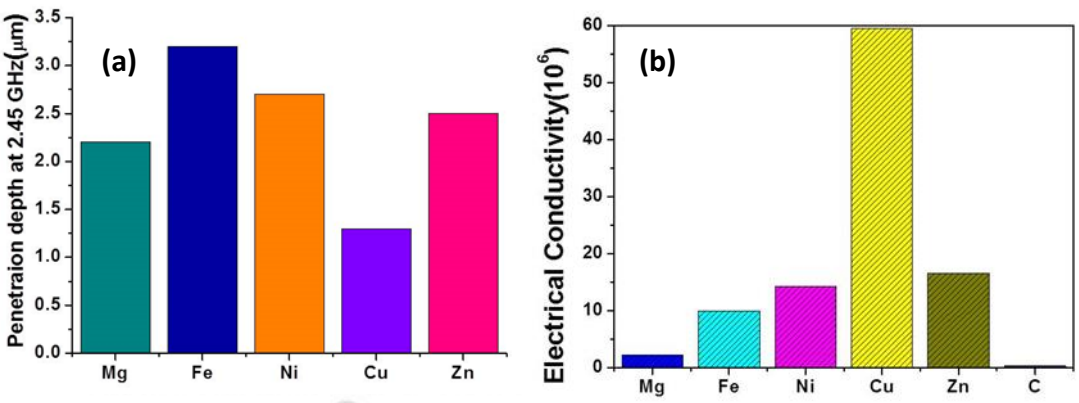

Figure 1.14 (a) Penetration depth and (b) electrical conductivity of selected materials such as, Mg, Fe, Ni, Cu, Zn, and Carbon [52].

1.4.4 Conduction losses for conductivity materials [47]

Insulating materials are hard to be heated at room temperature and they are transparent to microwaves such as oxide ceramics. As the temperature increases, the conductivity of these ceramics increases but resistivity decreases. This leads to an increase in the dielectric properties agree to enhance coupling with microwave. As well, inclusions of certain material may well provide a catalytic result and increase the

coupling of the material to microwaves. For instance, it has been presented that the addition of lesser amounts of metal powders can raise the microwave absorption and increases the reaction rate in solid-state reactions. The eddy currents or magnetic induction performance an imperative role in the heating of high conductivity materials. The eddy current was made inside the conductor because the interaction of the magnetic field produces a force that drives the conducting electrons external into a narrow area close the surfaces. The eddy current density decreases declarative with increasing depth that is known as the skin effect. The skin depth for conductors is set by **Eq. (1.7).** The use of the magnetic field to talk into eddy currents in the material forms the basis for orientation heating of metals [47-51].

1.4.5 Required power for increasing temperature

The power ($P_{Absorbed}$) required to increasing the temperature of mass, m (kg) of material from a primary temperature T_0 to T in time (t) seconds can be set by

$$P_{Absorbed} = \frac{mc_p(T - T_0)}{t} \quad \text{.....(1.10)}$$

Take the place of **Eq. (1.2)** for the power absorbed by the material into **Eq. (1.10)**, $\Delta T/\Delta t$, the rate of increase in temperature of the material, can be represented as

$$\frac{\Delta T}{\Delta t} = \frac{P_{Absorbed}}{\rho c_p} = \frac{2\pi f \varepsilon_0 \varepsilon_{eff}^{"} E_{rms}^2}{\rho c_p} \quad \text{.....(1.11)}$$

T is the temperature of system, t is the time (seconds), ρ is the material density and c_p is the specific heat of the material [47-51].

1.5 Metal Oxide for Gas Sensor and UV Sensor Devices

1.5.1 Metal oxide semiconductors [42, 53, 54]

In fifty years ago, Taguchi et al. is the first researcher group that firstly reported about the generation of the metal oxide semiconductors (MOSs) gas sensors were based on SnO_2 thick films since 1960s[42]. The metal oxide semiconductors had been literate in electrical diverse field of the gas sensors for widespread applications. The gas sensor was a detector device that could be used to detect a variety of gas for example ethanol, acetone, CO_2, LPG, and CO gases etc. the metal oxide semiconductors gas sensor for

example ZnO, TiO_2, SnO_2, In_2O_3, and WO_3 had an significant role in the chemical process for controlling, the environmental monitoring, the personal safety[55, 56], for the warning and protection of hazardous gas leaks, for the detection of toxic gases in the environmental pollutants, Medical examination of breath, food quality monitoring and traffic safety for driving. The MOS gas sensors devices fast gained interest over the years due to they have some good point such as small size, simple construction, low-power-consumption, good sensing properties, and high compatibility with the microelectronic processing[55, 56].

Recently, the MOSs has a number of morphologies of nanostructures for example rod-like, wire-like, belt-like, and tetrapods had been extensively investigated for the gas sensor applications devices. It had the sensitivity characteristics of these the sensors powerfully depend on the MOS nanostructures morphology. Especially, one-dimensional nanostructures for example nanorods, nanowires and nanobelts, had gained variously interest for nanoengineering and fabrication [57]. MOS nanostructures are hopeful for the gas sensor applications because of possibility for the ultrahigh sensitive of gas sensors or ppb-level sensors. There are a lot of reports about the gas sensor based on the nanostructures. They can be prepared by a number of method for example chemical vapors deposition (CVD), pulse laser deposition (PLD), and thermal oxidation technique.

1.5.2 Metal oxide semiconductors gas sensing fundamental mechanism

The gas sensing fundamental mechanism based on the metal oxide semiconductors depend on the reaction among first, the complexes of surface for example OH^-, H^+, O^{2-}, and O^- reactive of the chemical species and second, reducing or oxidizing gas of the gas molecules to be detected. Therefore, it was significant to understand of the surface reactions among MOS surface and objective gas for improved the gas sensing respond characteristics [42, 56, 58-60].

Typically, the sensor devices have the important parameter for developments are the sensitivity, the stability, and the selectivity that called “3S”[42]. Though, in this the chapter, the sensitivity parameter will most discuss on only. So, the parameter of sensitivity improvement had been at length studied by using very methods such as using

nanostructures that had been proved to be exceptional contenders for ultrahigh sensitivity because of their high surface-to-volume ratio[42], and Adding noble metal for example Au, Ag, Pt, and Pd on the surface of the metal oxide semiconductors able to act as a catalyst to change surface reactions of it toward detecting gas and end product in high sensitivity. Sensitivity (*S*) is present defined as the ratio of change R_a that the value of resistance the sensor before passing gas in air and R_g is after passing target gas and success the saturation value, also defined by the formula in **Eq. 1.12**[42, 61].

$$s = \frac{\Delta R}{R_a} = \left| \frac{R_a - R_g}{R_g} \right| \quad \text{.....(1.12)}$$

1.5.3 Sensing mechanism of the metal oxide semiconductors gas sensor

The sensing mechanism of the metal oxide semiconductors in target gas can explant by these concept processes. Usually, the metal oxide semiconductors gas sensor devices have an optimum operating temperature at the high temperature around from 250 to 350°C. When the metal oxide semiconductors is heated at the lesser temperature approximately100 to 200°C, the oxygen molecules be in the atmosphere are adsorbed around on it has surface and then form oxygen ion molecules by attracting an electron from the conduction band (CB) of the metal oxide semiconductors surface as presented in the **Eq. 1.13** [42].

$$O_2(Gas) + e^- \leftrightarrow O_2^-(Absorb) \quad \text{.....(1.13)}$$

At the upper temperature then the oxygen ion molecules are shown in **Eq. 1.14**[42] and (3) and dissociated into an oxygen ion atoms with one by one or twice as negative electric charges by appeal to an electron over again from the conduction band.

$$\tfrac{1}{2} O_2 + e^- \overset{k_{Oxy}}{\leftrightarrow} O_{ads}^- \quad \text{.....(1.14)}$$

$$\tfrac{1}{2} O_2 + 2e^- \overset{k_{Oxy}}{\leftrightarrow} O_{ads}^{2-} \quad \text{.....(1.15)}$$

Where, k_{Oxy} refer the reaction rate constant. Then the oxygen ions are exceedingly active with the objective gas molecule on the surface of MOS and transfer the electrons

(e^{-1}) from the surface get back to the conduction band. In a general chemical reaction between oxygen ions and gas molecule is shown in **Eq. 1.16**[42]**.**

$$X + O_{ads}^{V-} \xrightarrow{k_{gas}} X' + Ve^{-} \quad \text{.....(1.16)}$$

Where X and X' imply objective gas also out gas, respectively, the V value implies the amount of electron and k_{gas} imply the reaction of rate constant of the gas reaction. The chemical reactions motive the change of the concentration of transporter in the conductivity and so, change of the sensor resistance.

The changes of sensor resistance have two types of MOSs. The type of change of the sensor above exposure to resistance under the objective gas (reducing gas) in the event of p-type and n-type of the metal oxide semiconductors sensors was shown in the **Fig. 1.15** that will be respected in the next [42].

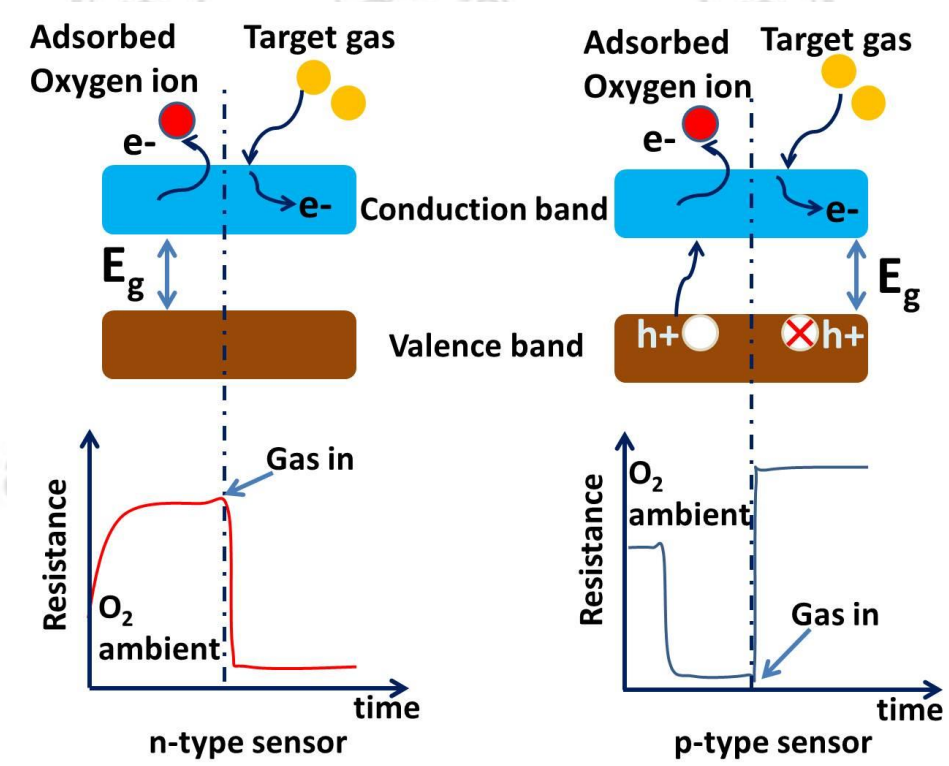

Figure 1.15 The schematic diagram for change of the event of p-type and n-type of the MOS sensor resistance [42].

Due to their semiconducting properties, the resistance of the n-type sensor reduced when the temperature enhance. But, under the oxygen ambient, was shown

from the **Eq. 1.13-1.15,** the electrons of the n-type in the conduction band are removed by the adsorbed oxygen ions. This motive the carrier concentration decrease and so, the resistance of the n-type sensor increases at working temperature. When the sensor of n-type be in the objective gas ambient or reducing gas, the electrons achieved from the chemical reaction that shown in the **Eq. 1.16** are given get back to the electrons to the conduction band bring about to a reduce of the sensor resistance [42].

On another hand, the widely held carriers in the p-type sensor are holes. The sensor resistance of the p-type sensor drops when the temperature enhances. Though, under ambient the oxygen, the p-type sensor generates the holes when the oxygen ions are adsorbed via the excited electrons beginning valence band on the surface. This procedure effects in raising the amount of the charge carriers, which bring about to reduces of the p-type sensor resistance that differing to n-type. When the p-type sensor is in the objective gas ambient (reducing gas), the electrons injected into the valence band and it recombines with the holes. This process brings about in decreasing the amount of holes [42].

The case of the oxidizing gas a change of resistance of the p-type sensor will be just opposite to directly above discussions the equation form. Moreover, we known that from the **Eq. 1.16**[42] and a rate equation form of the electron density able to be written as

$$\frac{dn}{dt} = k_{Gas}[O_{ads}]^V[X]^V \quad \text{.....(1.17)}$$

where n imply the density of electron that the electron concentration within the gas ambient, and k_{Gas} imply the reaction rate constant and/or else reaction rate of the coefficient described as

$$k_{Gas} = Ae^{(\frac{-E_a}{k_B T})} \quad \text{.....(1.18)}$$

Where E_a imply the activation energy of the reaction, T implies absolute temperature and k_B implies the Boltzmann constant. The **Eq. 1.17**[42] was integrated at the equilibrium state within the gas atmosphere and the air and the carrier concentration

was used to define as *n as α/R* (where *R* imply a resistance and *α* imply a proportional constant), the sensitivity (s) relation can be got as [42]

$$n = \Gamma_t k_{Gas} [O_{ads}^{Ion}]^V [X]^V + n_0 \quad \text{..... (1.19)}$$

$$S = \frac{R_a}{R_g} = \frac{\Gamma_t k_{Gas} [O_{ads}^{Ion}]^V [X]^V}{n_0} + 1 \quad \text{..... (1.20)}$$

Every so often, the sensitivity compact format of relation on the gas concentration, *X*, able to be revised as

$$S = aX^V + 1 \quad \text{..... (1.21)}$$

where *a* imply the controllable parameter.

The sensitivity formula that shown in the **Eq. 1.20**[42] able to be applicable to explain in the event of bulk, thin film and nanostructure, though, two important parameters along with the surface to volume ratio and depletion layer extensiveness must to think through in order explaining the characteristics of gas sensing.

1.5.4 Ultraviolet (UV) sensor

The ultraviolet (UV) radiant is ingredient of the radiation of electromagnetic spectrum in the **Fig 1.1**6 that it has high wavelength and the spectral range begin from the visible part (ca. 3.1 eV and 400 nm) and achieve the X-ray inferior wavelength and spectral low energy frontier (ca.124 eV and 10 nm) [62-67]. There are four spectral range regions of the ultraviolet radiation that emitted from the sun such as the UVA band (ca. 320–400 nm) light that the longest wavelength able to reach the earth's surface. The UVB band (ca. 280–320 nm) light that human skin able to be decently protected is absorbed by the molecules in sunscreens. The UVC band (ca. 200 to 280 nm) radiant is thoroughly absorbed that before it reach surface of the earth by the earth's atmosphere [ ]. The far UV spectrum that to be found in the range 10 to 200 nm wants an advanced level of the vacuum to spread, and for that cause is very usually entitled "vacuum UV". UVA can reach surface of the earth about 98.7% of the UV radiation [62-67].

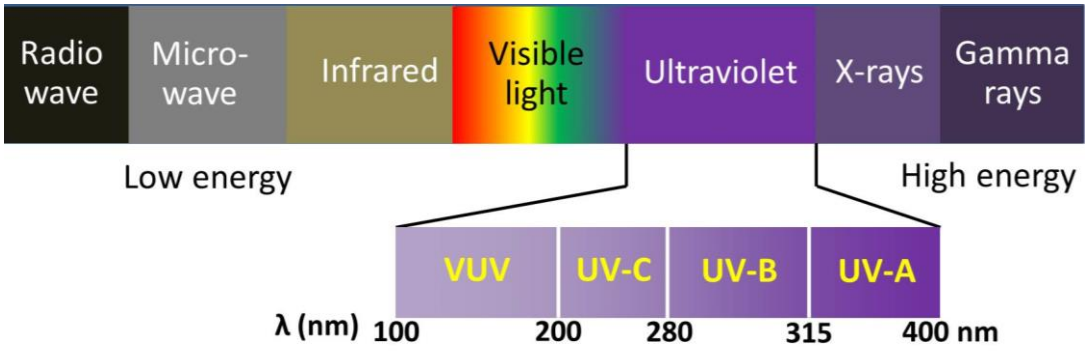

Figure 1.16 the schematic diagram of electromagnetic radiation spectrum for ultraviolet (UV) light is ingredient [62-67].

There are various research has shown that UVA light possibly will cause skin cancer. Then, the improvements of novel in effect ultraviolet sensor that show high UVA sensitivity however are blind just before standard visible radioactivity is of great significance. The ideal UV sensor for such applications is designed to exhibition in height responsivity, a well linearity of the photocurrent, a low noise level, and advanced selectivity. In addition, for high sensitivity presentation, these devices must to be chilled to decrease the dark current. For the example, UV respond is shown in the **Fig. 1.17** [68].

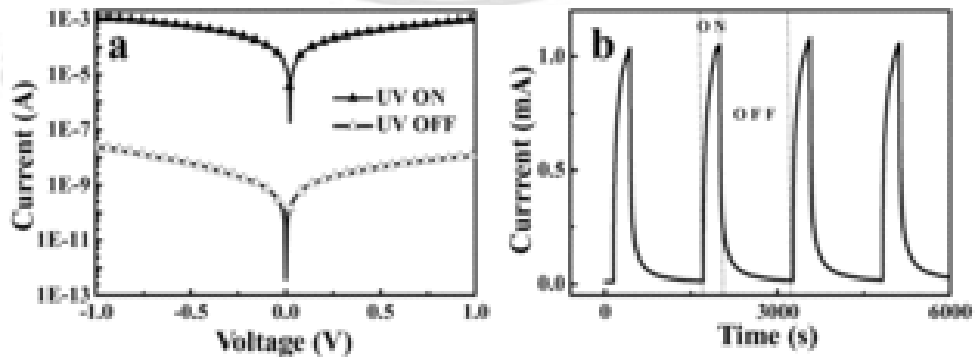

Figure 1.17 (a) IV curves of UV sensor nanowire with and without UV light. (b) Responsivity of the UV sensor nanowire within UV light of 4.5 $mWcm^{-2}$ and was

biased voltage of 1 V. Reprinted with permission from ref [68]. Copyright (2011) John Wiley and Sons.

Recently, wide band gap semiconducting oxide the have formation of the nanostructures such as TiO_2, ZnO, and SnO_2 have attracted great research attention because of their ultraviolet sensor and their optical transparency in the visible light of the spectral range and low-dimensional (LD) for UV sensor has attracted intense attention in **Fig.1.18** [11]. The synthesized LD nanostructure that was integrated with the electrical has been achieved with optical measures, which greater device versatility and promises high speeds. These wide band gap semiconductor that have nanostructures formation, for example quantum dots, nanobelts, nanotubes, nanorods, nanowires, and nanostructure arrays, are prospective to show key roles in UV sensor. Compared with UV sensor property based on traditional thin-film nanostructures and bulk materials, UV sensor based on the nanostructures commonly have an improvement of upper respond and photoconductivity gain due to their high surface-area-to-volume ratios and the decrease dimension of the effective electrical conductive channel [27, 68, 69].

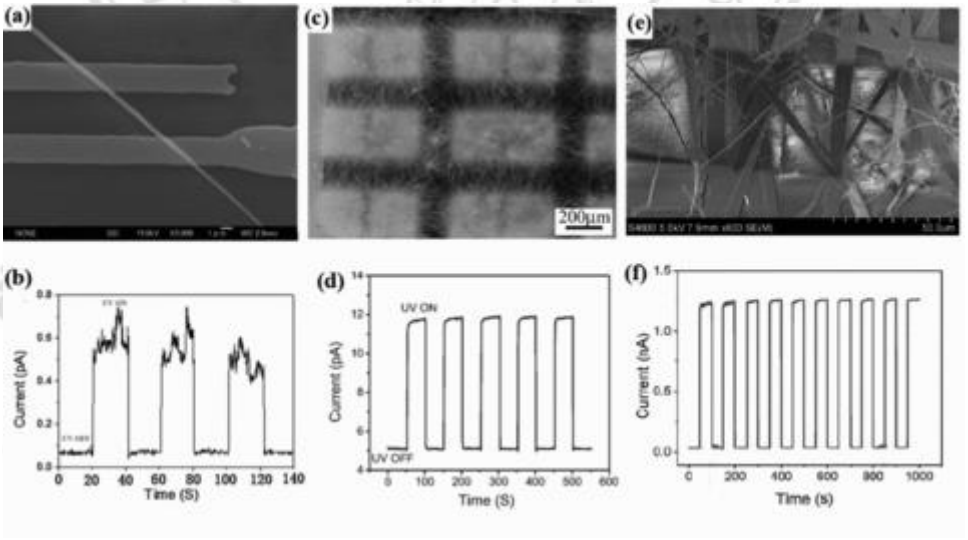

Figure 1.18 The corresponding time responses of the UV sensor of the ZnS nanostructures based on UV light sensor by the current measure further down and devoid UV illuminate: a, b) single ZnS nanobelt-based sensors, c, d) various ZnS-nanobelts, and, e and f) micro-scale ZnS nanobelt–based sensors. Reprinted with permission from ref [11]. Copyright (2013) John Wiley and Sons.

1.6 Literature review

Nanotechnology [1, 2, 7, 8] has been considered to be a breakthrough great technology which is promissing for a great impact to science community, electronic, medicine and industrial revolution. This is mainly due to novel and different properties about the physical and chemical properties of nanomaterials[13-15] as a result of reduction in size and increment in surface of volume which could open for new generation and fabrication of nanodevices[5] in a wide range of applications[28]. In addition, nanostructures or shapes of nanomaterials also play an important role for this emerging development [13-15].

The ZnO semiconductor material has caught attention due to their wide-ranging variety of structures or morphologies such as nanowires[55, 59], nanobelts [20, 21], nanoparticles[15], and tetrapods[27], which maybe the richest family in the middle of all materials in both structures and properties. For over the past decade, the nano-engineering[28], of the ZnO material by monitoring it has dimensions and morphology using a number of synthetic methods have been performed and a great multiplicity of nanostructured ZnO morphologies[1, 2, 7, 8] have been accomplished. The morphological variety of nanostructured ZnO material leads to a number of motivating properties together with surface-related[33] and opto-electrical[30-32] properties. In consequence, monitoring the growth kinetics of synthetic procedure via nano-engineering ZnO is an important issue for make use of ZnO nanostructures material [10, 34, 35].

In this work, we have controlled the growth kinetics of ZnO nanostructures by via a microwave-assisted thermal oxidation for synthesizing ZnO nanostructures morphologies. With this easily method and fast process, we have realized a unique the nanostructured ZnO morphology of material having the tetrapod-like features with leg-to-leg linking together, so known as ZnO Tetrapods Network or “interlinked ZnO tetrapod networks (ITN-ZnO)”. In addition, this ITN-ZnO as well exhibited without prior notice properties of electrical value and gas sensing properties when compared to other morphologies of ZnO structured. We have demonstrated the examples for potential applications in UV sensors and room temperature (RT) gas sensor.

1.7 Research Objectives and Usefulness of the Research

1.7.1 Research Objectives

A: To synthesize and characterize ZnO tetrapods network by using microwave assisted thermal oxidation technique.

B: To fabricate the gas sensing devices using the interlinked ZnO tetrapod networks as the sensing materials and examine theirs UV, ethanol, and acetone sensing properties.

1.7.2 Usefulness of the Research

1. This research may provide a technique for the preparation of nanostructures, which can be applied to other materials.

2. This research may provide preparation method and information of interlinked ZnO tetrapod networks that can be used for further applications.

3. The fabrication of gas sensing devices using the interlinked ZnO tetrapod networks may be useful for other sensing and electronic devices.